

Directional Detection of Dark Matter with 2D Targets

Yonit Hochberg^{1,2,*}, Yonatan Kahn^{3,†}, Mariangela Lisanti^{3,‡}, Christopher G. Tully^{3,§} and Kathryn M. Zurek^{1,2¶}

¹*Ernest Orlando Lawrence Berkeley National Laboratory, University of California, Berkeley, CA 94720*

²*Department of Physics, University of California, Berkeley, CA 94720 and*

³*Department of Physics, Princeton University, Princeton, NJ 08544*

We propose two-dimensional materials as targets for direct detection of dark matter. Using graphene as an example, we focus on the case where dark matter scattering deposits sufficient energy on a valence-band electron to eject it from the target. We show that the sensitivity of graphene to dark matter of MeV to GeV mass can be comparable, for similar exposure and background levels, to that of semiconductor targets such as silicon and germanium. Moreover, a two-dimensional target is an excellent directional detector, as the ejected electron retains information about the angular dependence of the incident dark matter particle. This proposal can be implemented by the PTOLEMY experiment, presenting for the first time an opportunity for directional detection of sub-GeV dark matter.

Introduction. The Weakly Interacting Massive Particle (WIMP) is currently the dominant theoretical paradigm for dark matter (DM), and has guided experimental search efforts in recent decades. Direct detection experiments, which search for DM-nucleus collisions, are currently targeting the WIMP parameter space [1–7]. However, null results from these searches motivate renewed consideration for a broader range of DM models. One possibility involves DM particles below the \sim GeV scale, which arise in a variety of theory scenarios [8–21]. Current direct detection experiments lose sensitivity to sub-GeV DM because the nuclear recoil energy is too small to be detected. However, DM with mass below a target nucleus deposits a greater fraction of its kinetic energy on an electron than a nucleus, making electrons a favorable target for light DM detection.

Consider the case of MeV-scale DM, which carries about an eV of kinetic energy, enough to excite atomic electrons after scattering [22]. The first limits on such processes have been set using data from the Xenon10 experiment [23]. The energy gap for electronic excitations in noble gases is ~ 10 eV, which places a lower bound on the DM mass that can be probed with these methods. However, a smaller energy deposit can up-scatter valence electrons in semiconductors with band gaps ~ 1 eV [22, 24]. As a result, semiconductor targets are more sensitive to DM in the 1–10 MeV mass range [25, 26]. Superconducting targets with \sim meV energy gaps are capable of reaching \sim keV masses [27, 28].

This Letter proposes an alternative approach using two-dimensional (2D) materials as targets. In this setup, an incident DM particle can deposit sufficient energy on a valence electron to eject it from the target. The energy and direction of the recoiling electron is then directly measured with a high-resolution calorimeter. This is in contrast to scattering in bulk targets, where the scattered particle (nucleus or electron) produces secondary excitations before measurement [2, 25, 26, 29], erasing the initial directional information in the scattering. Using 2D targets, DM masses down to the MeV scale can be probed

if the energy required to eject the electron is a few eV. As we will show, the PTOLEMY experiment [30], based at the Princeton Plasma Physics Laboratory, can realize this proposal with up to 0.5 kg of monolayer graphene, yielding competitive sensitivity to semiconductor targets.

Most importantly, 2D targets allow one to measure the direction of the incoming DM because the differential cross section for the outgoing electron is peaked in the forward direction. The lattice structure of the target can even yield diffraction patterns in the electron angular distribution for certain kinematics. Directional detection has long been recognized as a powerful tool in the study of DM, both as a discriminator against background sources and also because it leads to a daily modulation of the signal rate [31]. There are currently no feasible proposals for directional detection of sub-GeV DM [32], making the use of 2D targets a powerful tool in pushing sensitivities to lower DM masses.

Dark matter scattering in graphene. As a concrete example, we focus on monolayer graphene as a target. If the electron is ejected from the material, then its final-state wavefunction is well-modeled by a plane wave. The initial-state wavefunction corresponds to an electron in any of graphene’s four valence bands.¹ Analytic solutions for these wavefunctions in the tight-binding approximation are tractable due to the symmetries of the lattice [33], making this a convenient system in which to study DM scattering.

Monolayer graphene consists of carbon atoms arranged in a two-dimensional honeycomb lattice (Fig. 1). The distance between neighboring carbon atoms is $a = 0.142$ nm. The lattice is built from two distinct triangular sub-lattices. Four out of the six electrons of a carbon atom are valence electrons, occupying $(2s)(2p)^3$ orbitals. The 2s orbital becomes ‘hybridized’ with the in-plane p_x

¹ The core 1s electrons have binding energies of several hundred eV and contribute negligibly to the scattering rate.

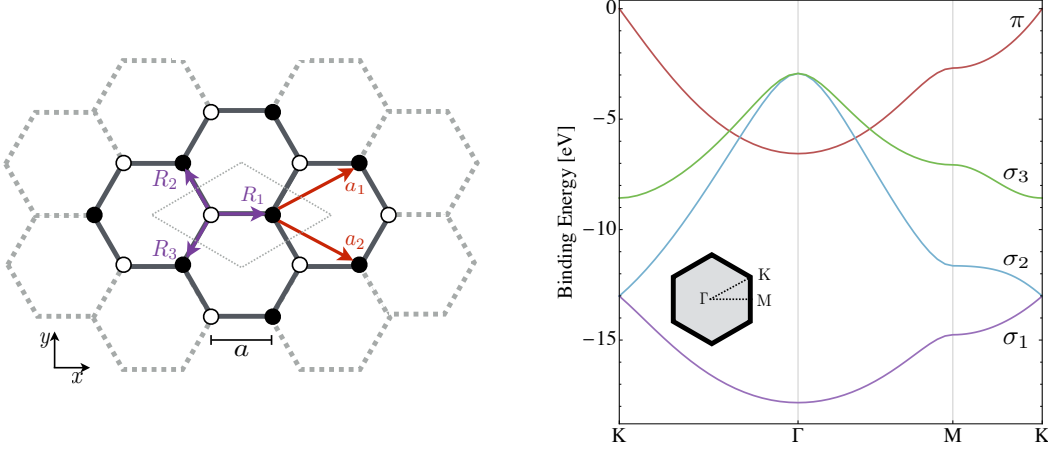


FIG. 1: (left) Graphene is comprised of two triangular carbon sub-lattices, which are illustrated by the open and solid circles. The lattice vectors $\mathbf{a}_{1,2}$ are indicated by the red arrows, and the nearest-neighbor vectors $\mathbf{R}_{1,2,3}$ are shown in purple. The gray diamond depicts the unit cell. The nearest-neighbor distance is $a = 0.142$ nm. (right) The valence-band diagram for graphene, as determined from the procedure outlined in the Appendix. The Brillouin zone is shown in the inset, with the high-symmetry points Γ , K , and M labeled.

and p_y orbitals, such that the energy eigenstates (called σ bonds) are linear combinations of $2s$, $2p_x$, and $2p_y$. The out-of-plane p_z orbitals remain unhybridized and form covalent bonds, called π . We outline the important features of the unhybridized π electron wavefunction here, relegating further details and a discussion of the σ electrons to the Appendix.

Within the tight-binding model, we approximate the wavefunction by a sum over nearest neighbors, corresponding to four lattice sites. The Bloch function for a π electron is given by

$$\Psi_\pi(\ell, \mathbf{r}) \approx \mathcal{N}_\ell \left(\phi_{2p_z}(\mathbf{r}) + e^{i\varphi_\ell} \sum_{j=1}^3 e^{i\ell \cdot \mathbf{R}_j} \phi_{2p_z}(\mathbf{r} - \mathbf{R}_j) \right) \quad (1)$$

for lattice momentum $\ell = (\ell_x, \ell_y) \in \text{BZ}$ in the Brillouin zone (inset of Fig. 1, right). Here, \mathcal{N}_ℓ is a normalization constant, \mathbf{R}_j are the nearest-neighbor vectors, and φ_ℓ is an ℓ -dependent phase. We take a hydrogenic orbital for the $2p_z$ wavefunction of carbon,

$$\phi_{2p_z}(\mathbf{r}) = \mathcal{N} a_0^{-3/2} \frac{r}{a_0} e^{-Z_{\text{eff}} r / 2a_0} \cos \theta, \quad (2)$$

where a_0 is the Bohr radius and \mathcal{N} is the normalization. The effective nuclear charge $Z_{\text{eff}} \simeq 4.03$ is chosen to fit the numerical solution for the overlap between adjacent $2p_z$ orbitals. The Fourier transform of Eq. (1) is

$$\tilde{\Psi}_\pi(\ell, \mathbf{k}) = \mathcal{N}_\ell (1 + e^{i\varphi_\ell} f(\ell + \mathbf{k})) \tilde{\phi}_{2p_z}(\mathbf{k}), \quad (3)$$

where \mathbf{k} is the momentum conjugate to \mathbf{r} , $f(\ell + \mathbf{k})$ is a sum of phase factors (defined in the Appendix),

and the Fourier transform of the atomic orbital is well-approximated by

$$\tilde{\phi}_{2p_z}(\mathbf{k}) \approx \tilde{\mathcal{N}} a_0^{3/2} \frac{a_0 k_z}{\left(a_0^2 |\mathbf{k}|^2 + (Z_{\text{eff}}/2)^2\right)^3} \quad (4)$$

with normalization $\tilde{\mathcal{N}}$. Note that the electron wavefunction has Fourier components at all \mathbf{k} values, as it is an energy eigenstate but not a momentum eigenstate.

Analytic forms for the σ electron wavefunctions are also possible to derive, but are more complicated than their π counterparts because the coefficients of the basis orbitals must be computed by diagonalizing a 6×6 Hamiltonian, as discussed in the Appendix. The π (σ_1) electrons have binding energies ~ 0 – 6 (13 – 18) eV, as shown in Fig. 1 (right).

The cross section for a DM particle of mass m_χ and initial velocity \mathbf{v} to scatter off an electron in band $i = \pi, \sigma_1, \sigma_2, \sigma_3$ with lattice momentum ℓ is

$$v \sigma_i(\ell) = \frac{\bar{\sigma}_e}{\mu_{e\chi}^2} \int \frac{d^3 k_f}{(2\pi)^3} \frac{d^3 q}{4\pi} |F_{\text{DM}}(q)|^2 \left| \tilde{\Psi}_i(\ell, \mathbf{q} - \mathbf{k}_f) \right|^2 \times \delta \left(\frac{k_f^2}{2m_e} + E_i(\ell) + \Phi + \frac{q^2}{2m_\chi} - \mathbf{q} \cdot \mathbf{v} \right), \quad (5)$$

where $-E_i(\ell)$ is the band energy, m_e is the electron mass, \mathbf{k}_f is the final electron momentum, \mathbf{q} is the momentum transfer, and $\mu_{e\chi}$ is the DM-electron reduced mass. $\Phi \simeq 4.3$ eV is the work function of graphene [34], defined as the energy difference between the Fermi surface

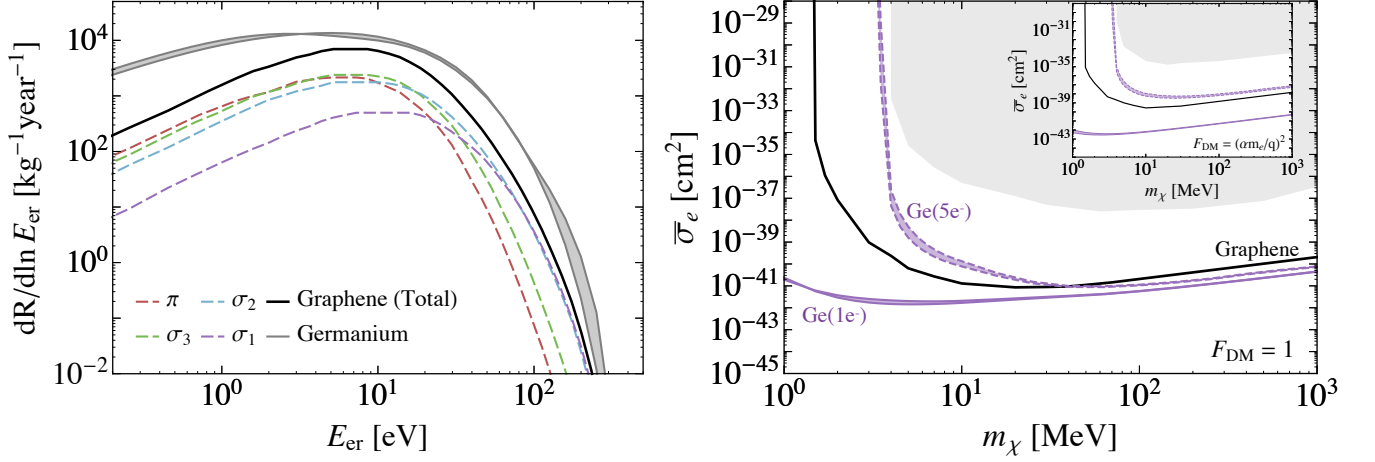


FIG. 2: (left) Differential rate for a 100 MeV DM particle scattering off an electron in graphene with $\bar{\sigma}_e = 10^{-37} \text{ cm}^2$ and $F_{\text{DM}}(q) = 1$. The solid black line denotes the total rate, while the dashed lines show the contributions for electrons in the individual π and σ bands. For comparison, the differential rate for germanium, taken from Ref. [25], is shown in gray; the band denotes the variation due to scattering off the 4s or 4p valence electron. (right) Expected background-free 95% C.L. sensitivity for a graphene target with a 1-kg-year exposure (black). Also plotted are the analogous curves for germanium [25] with 1-electron (solid purple) and 5-electron (dashed purple) thresholds including the variation due to 4s/4p bands, and exclusions from Xenon10 [23] (shaded gray). We consider both heavy-mediator exchange, which leads to $F_{\text{DM}}(q) = 1$, and light-mediator exchange, $F_{\text{DM}}(q) = (\alpha m_e / q)^2$ (inset).

and the vacuum.² Following Ref. [22], we define $\bar{\sigma}_e \equiv \frac{\mu_{e\chi}^2}{16\pi m_\chi^2 m_e^2} |\overline{\mathcal{M}_{e\chi}(q)}|^2_{q^2=\alpha^2 m_e^2}$, with $|\overline{\mathcal{M}_{e\chi}(q)}|^2$ the spin-averaged amplitude, to be the scattering cross section for DM off a free electron with $q = \alpha m_e$. The momentum dependence of the matrix element is then absorbed into the DM form factor $F_{\text{DM}}(q) = |\overline{\mathcal{M}_{e\chi}(q)}|/|\overline{\mathcal{M}_{e\chi}(\alpha m_e)}|$. We do not include the so-called Fermi factor, which enhances the rate at low recoil energies due to the distortion of the outgoing electron wavefunction by the Coulomb field of the nucleus. This factor is significant for bulk materials, but negligible for a 2D material for two reasons: the ionized electron energy must be high enough to overcome the work function, and the ionized electron travels single-atom distances and thus spends little time in the vicinity of the nucleus.

To obtain the total rate per unit time and detector mass, we must integrate Eq. (5) over all $\ell \in \text{BZ}$ and all incoming DM velocities, then sum the contributions from the four valence bands:

$$R = 2 \sum_{i=\pi, \sigma_{1,2,3}} \frac{\rho_\chi}{m_\chi} N_C A_{\text{uc}} \int \frac{d^2 \ell}{(2\pi)^2} d^3 v g(\mathbf{v}) v \sigma_i(\ell), \quad (6)$$

where $g(\mathbf{v})$ is the DM velocity distribution, $A_{\text{uc}} =$

$3\sqrt{3}a^2/2$ is the area of the unit cell, $N_C \simeq 5 \times 10^{25} \text{ kg}^{-1}$ is the density of carbon atoms in graphene, and $\rho_\chi \simeq 0.4 \text{ GeV/cm}^3$ is the local DM density [36]. The factor of two in Eq. (6) accounts for the degenerate spin states in each band.

The kinematics of the scattering process dictate that there is a minimal DM velocity required to eject an electron of momentum k_f from the target via a momentum transfer q :

$$v_{\text{min}}^i(\ell, k_f, q) = \frac{E_{\text{er}} + E_i(\ell) + \Phi}{q} + \frac{q}{2m_\chi}, \quad (7)$$

where $E_{\text{er}} \equiv k_f^2/2m_e$. For an electron at the Fermi surface with $E_i(\ell) = 0$, the minimum q needed for $v_{\text{min}} = v_{\text{esc}} = 550 \text{ km/s}$ is $q_{\text{min}} \simeq 2 \text{ keV}$. Comparing this with the inverse atomic spacing $2\pi/a \simeq 8.7 \text{ keV}$, we see that all kinematically allowed scattering is localized to only a few unit cells, with most confined to a single one. We have verified numerically for the π band that the nearest-neighbor approximation made in Eq. (1) is sufficient.

Rate results. We assume an isotropic velocity distribution $g(\mathbf{v}) = g(v)$ following the Standard Halo Model [37], with $v_0 \simeq 220 \text{ km/s}$ [38] and escape velocity $v_{\text{esc}} \simeq 550 \text{ km/s}$ [39]. Fig. 2 (left) shows the differential scattering rate for a 100 MeV DM particle. The total rate (solid black line) is comparable to that for a germanium target (gray band). The contributions from the individual π and σ electrons are indicated by the dashed lines. Although electrons in the lowest two σ bands contribute

² The work function is not an intrinsic property of graphene, and can be manipulated with a suitable choice of substrate; see *e.g.*, Ref. [35].

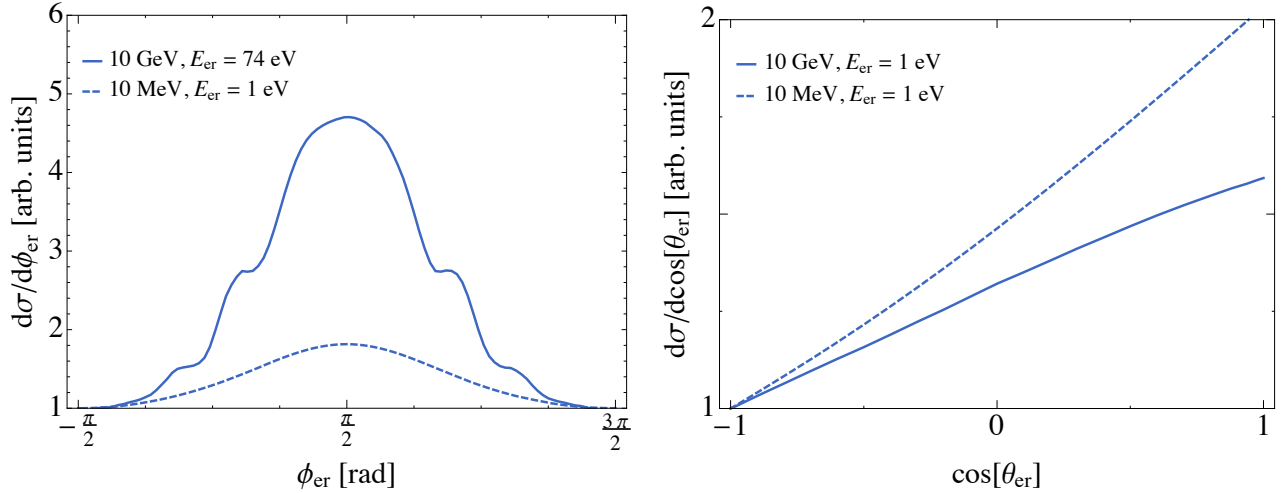


FIG. 3: (left) Azimuthal distribution of the final-state electron after scattering with a dispersionless DM stream with $v = v_{\text{esc}}$ that is oriented parallel to the graphene plane and points in the \hat{y} direction of $\phi = \pi/2$. The results are shown for 10 MeV (10 GeV) DM assuming an electron recoil of $E_{\text{er}} = 1$ (74) eV, indicated by the dashed (solid) line. (right) Polar distribution of the final-state electron, when the DM stream is perpendicular to the graphene plane and points in the \hat{z} direction of $\cos \theta = 1$. In this case, $E_{\text{er}} = 1$ eV for both mass examples.

the least at low recoil energies, they dominate at higher recoil energies. This is because the $\sigma_{1,2}$ bands are mostly 2s and therefore have a larger spread in momentum.

In the right panel of Fig. 2, we show the 95% one-sided Poisson C.L. expected reach (3.0 events) after 1-kg-year exposure of a graphene target, assuming a zero-background experiment. The reach is plotted for form factors of both heavy and light mediators, $F_{\text{DM}}(q) = 1$ and $F_{\text{DM}}(q) = (\alpha m_e/q)^2$, respectively. For comparison, we show the expected sensitivity of a germanium target [25] (with silicon performing similarly [26]). As is evident, graphene can be competitive with the reach of semiconductor targets over the \sim MeV–GeV DM mass range, depending on the threshold energy.

Directional detection. In a 2D material, DM can scatter electrons directly into the vacuum without additional interactions. Since scattering is primarily in the forward direction, the electrons retain information about the initial direction of the DM. This makes 2D targets especially suitable for directional detection. To illustrate this behavior, we consider the angular distribution of the scattered electron in graphene for the case of a dispersionless DM stream at the escape velocity, $g(v) \propto \delta(v - v_{\text{esc}})$, for streams parallel and normal to the graphene plane. The intuition afforded by these examples applies to generalized velocity distributions, which can always be broken down into parallel and normal components.

The left panel of Fig. 3 shows the azimuthal dependence of the scattering cross section for a DM stream oriented parallel to the graphene plane, pointing in the \hat{y} direction ($\phi = \pi/2$). The electrons are preferentially emitted in the same direction as the stream, for both 10 GeV

and 10 MeV DM masses. The heavier DM curve is plotted for $k_f = 2\pi/a \simeq 8.7$ keV ($E_{\text{er}} \simeq 74$ eV). A diffraction pattern is discernible in the angular distribution, arising from the interference between wavefunctions of neighboring carbon atoms. The diffraction pattern is washed out if the velocity dispersion of the stream is greater than ~ 25 km/s, but the scattering remains peaked in the forward direction. For the lighter DM, $k_f \sim 2\pi/a$ cannot be achieved at an appreciable rate, so the differential distribution is shown for $k_f = 1$ keV ($E_{\text{er}} \simeq 1$ eV). While no diffraction pattern emerges for recoil momenta small compared to the inverse lattice spacing, a broad forward-scattering peak persists. For streams in different in-plane directions, the shapes of the forward-scattering peak and the secondary peaks change, but the general features remain the same.

We emphasize that, for the directional information to persist, the electrons must exit the monolayer of the material without re-scattering. Thus, a DM stream in the plane of the material should eject electrons at a sufficiently large angle from the plane, restricting the phase space for directional detection. For example, if the DM exits at an angle greater than $\pi/4$ from the graphene plane, the rate corresponding to the 10 GeV diffraction distribution is reduced by a factor of 4.

The right panel of Fig. 3 shows the polar angular dependence of the scattering cross section for a DM stream normal to the plane, in the \hat{z} direction. The curves are plotted for $E_{\text{er}} = 1$ eV for both the 10 MeV and 10 GeV examples. As in previous examples, the differential rate is largest for forward scattering. Forward scattering is less favored for heavier DM because the mini-

mum kinematically-allowed q is smaller and the π wavefunction $\tilde{\phi}_{2p_z}(\mathbf{q} - \mathbf{k}_f)$ is suppressed when $q \sim k_f$ (see Eq. (4)).

Experimental Implementation. The PTOLEMY experiment [30] may offer a suitable experimental apparatus to search for MeV-scale DM. The primary goal of PTOLEMY is to detect electrons emitted from a tritium-loaded graphene surface after the capture of cosmic relic neutrinos. If the experiment is run using bare graphene surfaces (as would be done during a calibration run), it is also sensitive to DM scattering. When a scattered electron is ejected from the graphene surface, it enters into a crossed-field MAC-E filter that performs the same function as the KATRIN MAC-E filter [40] but implements an $\mathbf{E} \times \mathbf{B}$ configuration to allow parallel sheets of graphene to each be filtered individually in a compact geometry. This geometry is in the process of being implemented into the KATRIN Kasseiopeia simulation.

We expect the main irreducible background to be carbon-14 decay. Assuming the same $^{14}\text{C}/^{12}\text{C}$ ratio as obtained by Borexino [41], we conservatively estimate $\mathcal{O}(5)$ events/kg-yr for electrons with kinetic energy below 100 eV. Radon backgrounds may also pose a challenge, but the magnetic field should prevent most alpha particles from reaching the graphene. Other backgrounds that cause single-electron emission will need to be studied *in situ*.

Conclusions. This Letter presents a proposal for directional DM detection with 2D targets. If sufficient energy is deposited by the DM scattering, the electron can be ejected from the target and detected with a calorimeter. The electron retains information about its recoil direction, which is in turn correlated with the incoming DM direction. For a graphene target, this setup, which can be implemented by PTOLEMY, can probe DM down to MeV masses. The reach is comparable to that for semiconductor targets, with the added benefit of directionality. Further improvement can be made by lowering the graphene work function. Other 2D materials, such as monolayer gold [42], could be similarly powerful.

Advantageously, the same experiment can also be used to detect nuclear recoils, similar to proposals that have been made for carbon nanotubes [43, 44]. Only ~ 20 eV of energy is needed to eject a carbon atom from the graphene sheet (and slightly more to eject an ion) after scattering with the DM [45]. The ion can either be detected calorimetrically or by monitoring the conductivity of the graphene (see *e.g.*, [46, 47]). This would enable the same experimental setup to probe nuclear scattering down to $\sim \text{GeV}$ DM masses.

Lastly, 2D materials with a small band gap, such as graphene, may be sensitive to DM as light as the warm DM limit of $\sim \text{keV}$ masses. While small energy gaps and large target electron velocities have already been shown to allow superconductors to probe keV DM [27, 28], this target also exhibits a large optical response. Supercon-

ductors are thus limited in their sensitivity to scattering processes mediated by dark photons [28]. As a result, a material like graphene, with a weaker optical response, can be highly complementary to a superconducting target. We leave a detailed study of 2D targets for detection of keV–MeV DM for future work.

Acknowledgments. We thank Timothy Berkelbach, Garnet Chan, Youngkuk Kim, Andrew Rappe, and Joe Subotnik for enlightening discussions regarding graphene. We also thank Snir Gazit, Adolfo Grushin, Roni Ilan, Aaron Manalaysay, Dan McKinsey, Antonio Polosa, Matt Pyle, and Zohar Ringel for conversations about light dark matter detection in various materials. YH is supported by the U.S. National Science Foundation under Grant No. PHY-1002399. ML is supported by the DoE under contract DESC0007968, as well as by the Alfred P. Sloan Foundation. KZ is supported by the DoE under contract DE-AC02-05CH11231.

APPENDIX

This Appendix reviews the calculation of the analytic forms for the π and σ electron wavefunctions in graphene in the tight-binding approximation, which are needed for the determination of the scattering rate in Eq. (5). Our discussion follows Chap. 2 of Ref. [33] closely and we refer the interested reader there for a more comprehensive introduction.

The tight-binding Bloch wavefunction for an electron located on sub-lattice γ with periodic lattice momentum $\ell = (\ell_x, \ell_y)$ is

$$\Phi_\gamma(\ell, \mathbf{r}) = \frac{1}{\sqrt{N}} \sum_N e^{i\ell \cdot \mathbf{R}_N} \phi_s(\mathbf{r} - \mathbf{R}_N), \quad (\text{A1})$$

where the sum runs over N lattice sites s with position \mathbf{R}_N . In practice, we only sum over nearest-neighbor sites. For example, if the coordinate system is centered at an A site in the unit cell (open circle in Fig. 1), then the nearest neighbors consist of three B sites (solid circles) located at $\mathbf{R}_1, \mathbf{R}_2$, and \mathbf{R}_3 . The Bloch wavefunctions are then

$$\begin{aligned} \Phi_A(\ell, \mathbf{r}) &= \phi_A(\mathbf{r}) \\ \Phi_B(\ell, \mathbf{r}) &= \sum_{j=1}^3 e^{i\ell \cdot \mathbf{R}_j} \phi_B(\mathbf{r} - \mathbf{R}_j). \end{aligned} \quad (\text{A2})$$

Electrons in the π band are in the $2p_z$ atomic orbital of carbon. Therefore, $\phi_A(\mathbf{r}) = \phi_B(\mathbf{r}) = \phi_{2p_z}(\mathbf{r})$ because the A and B sites are both identical carbon atoms. The hydrogenic orbital for a $2p_z$ electron in carbon is

$$\phi_{2p_z}(\mathbf{r}) = 3.23 a_0^{-3/2} \frac{r}{a_0} e^{-Z_{\text{eff}} r / 2a_0} \cos \theta, \quad (\text{A3})$$

with a_0 the Bohr radius. We take the effective charge $Z_{\text{eff}} \simeq 4.03$ to reproduce the nearest-neighbor overlap $s = 0.129$ [33].

The wavefunction for a π electron in graphene is therefore

$$\Psi_\pi(\ell, \mathbf{r}) = C_A(\ell) \Phi_A(\ell, \mathbf{r}) + C_B(\ell) \Phi_B(\ell, \mathbf{r}), \quad (\text{A4})$$

where $C_{A,B}$ are constants that depend on ℓ . In the following, we will suppress their ℓ dependence for notational simplicity. This wavefunction must satisfy

$$H \Psi_\pi = E_\pi(\ell) \Psi_\pi, \quad (\text{A5})$$

where H is the crystal Hamiltonian and E_π is the energy of the π -band electron. Defining the vector $\mathbf{C} = (C_A, C_B)$, Eq. (A5) can be rewritten as

$$\mathcal{H} \mathbf{C} = E_\pi(\ell) \mathcal{S} \mathbf{C}. \quad (\text{A6})$$

Here, \mathcal{S} is the overlap matrix

$$\mathcal{S}_{\gamma\gamma'} = \langle \Phi_\gamma(\ell, \mathbf{r}) | \Phi_{\gamma'}(\ell, \mathbf{r}) \rangle, \quad (\text{A7})$$

which becomes

$$\mathcal{S} = \begin{pmatrix} 1 & sf(\ell) \\ sf(\ell)^* & 1 \end{pmatrix} \quad (\text{A8})$$

for the π electrons. The overlap between nearest-neighbor atomic orbitals is

$$s = \int d^3r \phi_{2p_z}^*(\mathbf{r}) \phi_{2p_z}(\mathbf{r} - \mathbf{R}_j) = 0.129. \quad (\text{A9})$$

Additionally, $f(\ell)$ is the phase factor

$$\begin{aligned} f(\ell) &= e^{i\ell \cdot \mathbf{R}_1} + e^{i\ell \cdot \mathbf{R}_2} + e^{i\ell \cdot \mathbf{R}_3} \\ &= e^{i\ell_x a} + 2e^{-i\ell_x a/2} \cos\left(\frac{\sqrt{3}\ell_y a}{2}\right), \end{aligned} \quad (\text{A10})$$

where $a = 0.142$ nm is the nearest-neighbor distance.

Similarly, the transfer matrix \mathcal{H} is defined in terms of the crystal Hamiltonian H as

$$\mathcal{H}_{\gamma\gamma'} = \langle \Phi_\gamma(\ell, \mathbf{r}) | H | \Phi_{\gamma'}(\ell, \mathbf{r}) \rangle, \quad (\text{A11})$$

and can be written as

$$\mathcal{H} = \begin{pmatrix} \epsilon_{2p} & tf(\ell) \\ tf(\ell)^* & \epsilon_{2p} \end{pmatrix}, \quad (\text{A12})$$

where the transfer integral t is

$$t = \int d^3r \phi_{2p_z}^*(\mathbf{r}) H \phi_{2p_z}(\mathbf{r} - \mathbf{R}_j) = -3.03 \text{ eV}. \quad (\text{A13})$$

By convention, the $2p$ orbital energy is set to the reference value $\epsilon_{2p} = 0$.

The energy eigenvalues are obtained by solving $\det[\mathcal{H} - E_\pi(\ell)\mathcal{S}] = 0$. The result is

$$E_\pi(\ell) = \frac{\epsilon_{2p} \pm t|f(\ell)|}{1 \pm s|f(\ell)|}, \quad (\text{A14})$$

where the plus sign corresponds to the valence π band and the minus sign corresponds to the conduction π^* band. The corresponding eigenvectors are

$$\mathbf{C}(\ell) = \frac{1}{\sqrt{2}} \begin{pmatrix} 1 \\ \pm e^{i\varphi_\ell} \end{pmatrix}, \quad \text{with } \varphi_\ell = -\arctan\left(\frac{\text{Im}f(\ell)}{\text{Re}f(\ell)}\right). \quad (\text{A15})$$

Thus, the complete expression for the π wavefunction is

$$\Psi_\pi(\ell, \mathbf{r}) = \mathcal{N}_\ell (\Phi_A(\ell, \mathbf{r}) + e^{i\varphi_\ell} \Phi_B(\ell, \mathbf{r})), \quad (\text{A16})$$

where \mathcal{N}_ℓ is a normalization constant.

For our rate calculation, we must also consider the σ electrons, which are in a superposition of the $2s$, $2p_x$, and $2p_y$ orbitals. Since these orbitals are even under reflection in the graphene plane while the $2p_z$ orbital is odd, there is a super-selection rule forbidding the π band from mixing with the σ bands, and we can diagonalize the σ electrons separately. To obtain the energies and wavefunctions for the σ electrons, we follow a similar procedure as for the π electrons. However, the calculation is now more involved as the transfer and overlap matrices are 6×6 when written in the $(2s^A, 2p_x^A, 2p_y^A, 2s^B, 2p_x^B, 2p_y^B)$ basis. For example, the AA sub-matrices are

$$\mathcal{S}_{AA} = \begin{pmatrix} 1 & 0 & 0 \\ 0 & 1 & 0 \\ 0 & 0 & 1 \end{pmatrix} \quad \text{and} \quad \mathcal{H}_{AA} = \begin{pmatrix} \epsilon_{2s} & 0 & 0 \\ 0 & \epsilon_{2p} & 0 \\ 0 & 0 & \epsilon_{2p} \end{pmatrix}, \quad (\text{A17})$$

where $\epsilon_{2s} = -8.87$ eV is the energy of the $2s$ orbital relative to $\epsilon_{2p} = 0$. The BB sub-matrices are identical to Eq. (A17). The AB sub-matrices are more complicated: for the overlap matrix, we have

$$\mathcal{S}_{AB} = \begin{pmatrix} \mathcal{S}_{ss} & \mathcal{S}_{sp_x} & \mathcal{S}_{sp_y} \\ -\mathcal{S}_{sp_x} & \mathcal{S}_{p_x p_x} & \mathcal{S}_{p_x p_y} \\ -\mathcal{S}_{sp_y} & \mathcal{S}_{p_x p_y} & \mathcal{S}_{p_y p_y} \end{pmatrix}, \quad (\text{A18})$$

with elements

$$\begin{aligned} \mathcal{S}_{ss} &= S_{ss} \left(e^{i\ell_x a} + 2e^{-i\ell_x a/2} \cos\left(\frac{\sqrt{3}\ell_y a}{2}\right) \right) \\ \mathcal{S}_{sp_x} &= S_{sp} \left(-e^{i\ell_x a} + e^{-i\ell_x a/2} \cos\left(\frac{\sqrt{3}\ell_y a}{2}\right) \right) \\ \mathcal{S}_{sp_y} &= -i\sqrt{3} S_{sp} e^{-i\ell_x a/2} \sin\left(\frac{\sqrt{3}\ell_y a}{2}\right) \\ \mathcal{S}_{p_x p_x} &= -S_\sigma e^{i\ell_x a} + \frac{(3S_\pi - S_\sigma)}{2} e^{-i\ell_x a/2} \cos\left(\frac{\sqrt{3}\ell_y a}{2}\right) \\ \mathcal{S}_{p_x p_y} &= \frac{i\sqrt{3}}{2} (S_\sigma + S_\pi) e^{-i\ell_x a/2} \sin\left(\frac{\sqrt{3}\ell_y a}{2}\right) \\ \mathcal{S}_{p_y p_y} &= S_\pi e^{i\ell_x a} + \frac{(S_\pi - 3S_\sigma)}{2} e^{-i\ell_x a/2} \cos\left(\frac{\sqrt{3}\ell_y a}{2}\right). \end{aligned}$$

S	value	\mathcal{H}	value (eV)
S_{ss}	0.21	H_{ss}	-6.77
S_{sp}	0.16	H_{sp}	-5.58
S_{σ}	0.15	H_{σ}	-5.04
S_{π}	0.13	H_{π}	-3.03

TABLE A1: Inputs for the transfer and overlap matrices [33].

The elements of the AB transfer matrix, \mathcal{H}_{AB} , can be constructed by replacing $S \rightarrow \mathcal{H}$ and $S \rightarrow H$ in Eq. (A18).

Table A1 shows the numerical values of the transfer and overlap matrices used in our calculation. S_{ss}, S_{σ} , and S_{π} are taken from Ref. [33]. Because the graphene plane breaks spherical symmetry, the Z_{eff} used in the $2p_z$ orbital need not be the same as for the other orbitals. For self-consistency, we choose the values of Z_{eff} for the $2p_x/2p_y$ and $2s$ orbitals separately to reproduce the values for S_{σ} and S_{ss} in Table A1: $Z_{\text{eff}}^{2p_x/2p_y} \simeq 5.49$ and $Z_{\text{eff}}^{2s} \simeq 4.84$. This fixes the functional form of all valence orbitals, and the resulting self-consistent value for the $2s/2p$ overlap S_{sp} is 0.163, which differs slightly from $S_{sp} = 0.10$ found in Ref. [33]. However, the uppermost σ band is unaffected by this change, and the effect on the lower two σ bands is at most 1 eV, so we do not expect this difference to appreciably affect the rate. The band structure for our choice of parameters is plotted in Fig. 1.

* Electronic address: yonit.hochberg@berkeley.edu

† Electronic address: ykahn@princeton.edu

‡ Electronic address: mlisanti@princeton.edu

§ Electronic address: cgtully@princeton.edu

¶ Electronic address: kzurek@berkeley.edu

- [1] E. Aprile et al. (XENON100), Phys. Rev. Lett. **109**, 181301 (2012), 1207.5988.
- [2] R. Agnese et al. (SuperCDMS), Phys. Rev. Lett. **112**, 041302 (2014), 1309.3259.
- [3] R. Agnese et al. (SuperCDMS), Phys. Rev. Lett. **112**, 241302 (2014), 1402.7137.
- [4] D. S. Akerib et al. (LUX), Phys. Rev. Lett. **116**, 161301 (2016), 1512.03506.
- [5] G. Angloher et al. (CRESST), Eur. Phys. J. **C76**, 25 (2016), 1509.01515.
- [6] R. Agnese et al. (SuperCDMS), Phys. Rev. Lett. **116**, 071301 (2016), 1509.02448.
- [7] E. Aprile et al. (XENON100) (2016), 1605.06262.
- [8] R. N. Mohapatra and V. L. Teplitz, Phys. Rev. **D62**, 063506 (2000), astro-ph/0001362.
- [9] R. N. Mohapatra, S. Nussinov, and V. L. Teplitz, Phys. Rev. **D66**, 063002 (2002), hep-ph/0111381.
- [10] C. Boehm and P. Fayet, Nucl. Phys. **B683**, 219 (2004), hep-ph/0305261.
- [11] M. J. Strassler and K. M. Zurek, Phys. Lett. **B651**, 374 (2007), hep-ph/0604261.
- [12] M. Pospelov, A. Ritz, and M. B. Voloshin, Phys. Lett. **B662**, 53 (2008), 0711.4866.
- [13] D. Hooper and K. M. Zurek, Phys. Rev. **D77**, 087302 (2008), 0801.3686.
- [14] J. L. Feng and J. Kumar, Phys. Rev. Lett. **101**, 231301 (2008), 0803.4196.
- [15] D. E. Kaplan, M. A. Luty, and K. M. Zurek, Phys. Rev. **D79**, 115016 (2009), 0901.4117.
- [16] K. M. Zurek, Phys. Rept. **537**, 91 (2014), 1308.0338.
- [17] Y. Hochberg, E. Kuflik, T. Volansky, and J. G. Wacker, Phys. Rev. Lett. **113**, 171301 (2014), 1402.5143.
- [18] Y. Hochberg, E. Kuflik, H. Murayama, T. Volansky, and J. G. Wacker, Phys. Rev. Lett. **115**, 021301 (2015), 1411.3727.
- [19] R. T. D’Agnolo and J. T. Ruderman, Phys. Rev. Lett. **115**, 061301 (2015), 1505.07107.
- [20] E. Kuflik, M. Perelstein, N. R.-L. Lorier, and Y.-D. Tsai, Phys. Rev. Lett. **116**, 221302 (2016), 1512.04545.
- [21] D. Pappadopulo, J. T. Ruderman, and G. Trevisan (2016), 1602.04219.
- [22] R. Essig, J. Mardon, and T. Volansky, Phys. Rev. **D85**, 076007 (2012), 1108.5383.
- [23] R. Essig, A. Manalaysay, J. Mardon, P. Sorensen, and T. Volansky, Phys. Rev. Lett. **109**, 021301 (2012), 1206.2644.
- [24] P. W. Graham, D. E. Kaplan, S. Rajendran, and M. T. Walters, Phys. Dark Univ. **1**, 32 (2012), 1203.2531.
- [25] S. K. Lee, M. Lisanti, S. Mishra-Sharma, and B. R. Safdi, Phys. Rev. **D92**, 083517 (2015), 1508.07361.
- [26] R. Essig, M. Fernandez-Serra, J. Mardon, A. Soto, T. Volansky, and T.-T. Yu, JHEP **05**, 046 (2016), 1509.01598.
- [27] Y. Hochberg, Y. Zhao, and K. M. Zurek, Phys. Rev. Lett. **116**, 011301 (2016), 1504.07237.
- [28] Y. Hochberg, M. Pyle, Y. Zhao, and K. M. Zurek (2015), 1512.04533.
- [29] R. Agnese et al. (SuperCDMS), Phys. Rev. **D92**, 072003 (2015), 1504.05871.
- [30] S. Betts et al., in *Community Summer Study 2013: Snowmass on the Mississippi (CSS2013) Minneapolis, MN, USA, July 29-August 6, 2013* (2013), 1307.4738.
- [31] D. N. Spergel, Phys. Rev. **D37**, 1353 (1988).
- [32] F. Mayet et al., Phys. Rept. **627**, 1 (2016), 1602.03781.
- [33] R. Saito, G. Dresselhaus, and M. S. Dresselhaus, *Physical Properties of Carbon Nanotubes* (Imperial College Press, 1998).
- [34] Puschnig, P. and Lüftner, D., J. of Electron Spectroscopy and Related Phenomena **200**, 193 (2015).
- [35] H. Yuan et al., Nano Letters **15**, 6475 (2015).
- [36] J. I. Read, J. Phys. **G41**, 063101 (2014), 1404.1938.
- [37] A. K. Drukier, K. Freese, and D. N. Spergel, Phys. Rev. **D33**, 3495 (1986).
- [38] P. J. McMillan and J. J. Binney, Mon. Not. Roy. Astron. Soc. **402**, 934 (2010), 0907.4685.
- [39] M. C. Smith et al., Mon. Not. Roy. Astron. Soc. **379**, 755 (2007), astro-ph/0611671.
- [40] G. Drexlin, V. Hannen, S. Mertens, and C. Weinheimer, Adv. High Energy Phys. **2013**, 293986 (2013), 1307.0101.
- [41] P. Mosteiro et al., Nucl. Part. Phys. Proc. **265-266**, 87 (2015), 1508.05379.
- [42] A. Drukier, K. Freese, A. Lopez, D. Spergel, C. Cantor, G. Church, and T. Sano (2012), 1206.6809.
- [43] L. M. Capparelli, G. Cavoto, D. Mazzilli, and A. D. Polosa, Phys. Dark Univ. **9-10**, 24 (2015), [Erratum: Phys. Dark Univ. **11**, 79 (2016)], 1412.8213.

- [44] G. Cavoto, E. N. M. Cirillo, F. Cocina, J. Ferretti, and A. D. Polosa (2016), 1602.03216.
- [45] A. Merrill, C. Cress, J. E. Rossi, N. D. Cox, and B. J. Landi, Phys. Rev. B. **92**, 075404 (2015).
- [46] F. Schwier, Nature Nanotechnology **5**, 487 (2010).
- [47] S. Sorgenfrei, C.-Y. Chiu, R. L. Gonzalez Jr, Y.-J. Yu, P. Kim, C. Nuckolls, and K. L. Shepard, Nature Nanotechnology **6**, 126 (2011).